Formation of porous metal oxides in the anodization process

C. Sample and A. A. Golovin
Department of Engineering Sciences and Applied Mathematics, Northwestern University, Evanston, Illinois 60208, USA
(Received 2 August 2006; published 26 October 2006)

A theory of the formation of nanoscale porous structures in oxides of metals grown by anodization is developed. It is shown that a growing oxide layer can become unstable which yields the formation of a spatially irregular array of pores. The instability is shown to result from a nonlinear dependence of electrochemical kinetics at the metal-oxide and oxide-electrolyte interfaces on the overpotential which is governed by the Butler-Volmer relation. The conditions for the instability of the oxide layer are found. The dependence of the oxide conductivity on the electric field is taken into account and is shown to have a destabilizing effect. A weakly nonlinear analysis is performed and it shows that the system evolution near the instability threshold is described by the Kuramoto-Sivashinsky equation. Farther from threshold, in the long-wave approximation, a system of strongly nonlinear equations is derived and solved numerically; this system describes the formation of deep irregular pores. In a particular case, a self-similar solution describing the propagation of a pore with a paraboloidal shape is found.

DOI: 10.1103/PhysRevE.74.041606 PACS number(s): 81.15.Aa, 82.45.Cc, 82.45.Yz, 89.75.Kd

I. INTRODUCTION

Spontaneous formation of nanoscale pores in an oxide layer growing at a metal-electrolyte interface during the metal anodization process was observed for several metals, such as aluminum [1,2], titanium [3–5], and tin [6]. The most striking example is self-assembly of spatially regular, hexagonally ordered arrays of nanoscale pores in aluminum oxide [7–10] that can be used as templates for fabrication of various nanostructures [11–14]. However, the formation of spatially ordered pores was observed only in alumina, under specific conditions [9,15,16], while irregular porous structures were observed to form more easily, in alumina [10,17], in oxides of other metals grown by anodization [3,4,6], as well as in anodically formed silica [18–20].

Despite a large number of experimental studies of the formation of nanoporous structures in anodic metal oxides, there were few theoretical studies of this process. In [21,22] a growth of a single pore was considered. Also, in [22] a model for the instability mechanism leading to the pore formation, based on field-assisted oxide dissolution, was proposed. The model formulated in [22] was recently further developed in [23,24]. It was shown that the oxide layer instability results from the positive feedback between the rates of electrochemical reactions at the oxide-electrolyte interface and the overpotentials, described by the Butler-Volmer relation. It was also shown that the wavelength selection mechanism, which determines the average pore diameter, can be associated with the effect of the surface energy on the electrochemical kinetics. Finally, a mechanism for the formation of spatially regular, hexagonally ordered pore arrays in aluminum oxide was proposed. It was shown that self-assembly of spatially regular patterns in this system can result from the effect of elastic stress in the growing oxide layer on the kinetics of electrochemical reactions.

The main factor that determines the formation of porous structures in a growing oxide is the spatial distribution of electric field inside the oxide layer. In [23,24] it was described by a Laplace equation for the electric potential that follows from the assumption of a constant electric conductivity of the oxide. However, the latter is determined by the migration of oxygen ions which is known to be an activated process that strongly depends on the applied electric field [25]. Also, the effect of overpotential on the rate of the oxidation reaction at the metal-oxide interface was neglected; although for aluminum this approximation is valid, it may be an oversimplification for other systems.

In this paper we present further development of the theory described in [23,24] and take into account two important effects: the nonlinear dependence of the oxide conductivity on electric field, and the effect of overpotential on the oxidation reaction at the metal-oxide interface. Also, we expand the nonlinear analysis developed in [24] and derive and numerically solve strongly nonlinear equations that can describe the formation of pores in the long-wave approximation far from the instability threshold.

II. FORMULATION OF THE PROBLEM

The model formulated here is a modification of the model formulated in [23,24]. Consider an electrolytic cell with a metallic anode in contact with an electrolyte. When a voltage is applied to the electrolytic cell, the metal surface undergoes anodization: it reacts with the electrolyte, which results in a layer of the metal oxide growing on the surface of the anode. Typically, after the formation, the growth of the oxide layer is sustained by the oxidation reaction that occurs due to electromigration of oxygen and hydroxyl ions through the oxide toward the metal-oxide (MO) interface. At the same time, dissolution of the oxide occurs at the oxide-electrolyte (OE) interface. The interfacial electrochemical reactions and the ion migration through the oxide layer are activated processes. Thus, the rates of electrochemical reactions at MO and EO interfaces, as well as the ion mobility, depend strongly on the applied voltage [25]. Since the conductivity of the oxide is much less than that of the metal and the electrolyte, we consider only the dynamics of the electric field in the oxide layer, assuming a constant voltage V at the metal side of the MO interface and a zero voltage at the electrolyte side of the OE interface.

We introduce a Cartesian coordinate system with the z axis normal to the initially planar oxide layer and in-plane

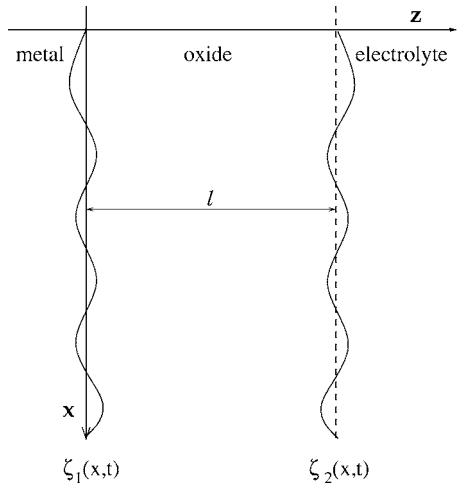

FIG. 1. System setting.

coordinates $\mathbf{x}=(x,y)$. The shapes of the MO and OE interfaces are described by $z=\zeta_1(\mathbf{x},t)$ and $z=\zeta_2(\mathbf{x},t)$, respectively (see Fig. 1). The dynamics of the system can be described by the following equations and boundary conditions for the electric potential in the oxide layer, $\phi(\mathbf{x},t)$, and the interfacial shapes $\zeta_{1,2}$:

$$\nabla\cdot[\sigma(E)\,\nabla\,\phi]=0, \tag{1}$$

$$z=\zeta_1(\mathbf{x},t):\quad -\sigma(E)\partial_n\phi=k_o e^{\alpha_e(V-\phi)}, \tag{2}$$

$$v_n^{(1)}=-b_o k_o e^{\alpha_e(V-\phi)}, \tag{3}$$

$$z=\zeta_2(\mathbf{x},t):\quad -\sigma(E)\partial_n\phi=k_d e^{\alpha_e\phi}-\bar{k}_d e^{-\alpha_e\phi}, \tag{4}$$

$$v_n^{(2)}=-b_d k_d e^{\alpha_e\phi}+\bar{b}_d\bar{k}_d e^{-\alpha_e\phi}. \tag{5}$$

Equation (1) describes the conservation of charge in the oxide layer, with the conductivity $\sigma(E)$ depending, according to [25], on the strength of the electric field, $E=|\nabla\phi|$,

$$\sigma(E)=\sigma_0 f(E)\equiv\sigma_0\frac{\sinh(pE)}{pE}, \tag{6}$$

where $p=\nu e/(k_B T)$. Here ν is the "activation length," e is the electron charge, k_B is the Boltzmann constant, and T is the absolute temperature [25]. The boundary conditions (2) and (4) are the Butler-Volmer relations [25] for the electron transfer reactions at the MO and OE interfaces, respectively, with k_o and k_d being the rates of metal oxidation and oxide dissolution, respectively, and $\bar{k}_d$ being the rate of the reaction inverse to dissolution (oxide reformation). The coefficient $\alpha_e=e/(2k_B T)$, where e is the electron charge and 1/2 is the so-called symmetry factor [25]. The rate constants k_o, k_d, and $\bar{k}_d$ depend on the concentration (pH) of the electrolyte, as well as on the curvature of the interfaces, due to the dependence of electrochemical reaction activation energies on the Laplace pressure, according to the transition state theory [26–28]. Thus, we set

$$k_o=k_o^0 e^{\gamma_o m_1},\quad k_d=k_d^0 e^{\gamma_d m_2},\quad \bar{k}_d=\bar{k}_d^0 e^{-\bar{\gamma}_d m_2}, \tag{7}$$

where $m_{1,2}$ are the mean curvatures of the interfaces $\zeta_{1,2}$ (positive for convex surfaces), and the positive parameters γ_0, γ_d, and $\bar{\gamma}_d$ are "activation capillary lengths," proportional to the derivatives of the corresponding activation energies with respect to the interfacial curvatures (see [24] for more details). Relations (7) describe a natural physical mechanism providing for a short-wave cutoff of the oxide layer instability (see below). Note, however, that other cutoff mechanisms, e.g., associated with some details of chemical kinetics at a curved interface, could also be possible [29]. The prefactors k_o^0, k_d^0, and $\bar{k}_d^0$ depend on the electrolyte pH which can be an important factor determining the morphology of the forming porous structures [5,20–22]; in the context of the present paper, however, we do not analyze this dependence. The boundary conditions (3) and (5) describe the motion of the interfaces due to electrochemical reactions. Here, ∂_n denotes the normal derivative,

$$v_n^{(1,2)}=\frac{\partial\zeta_{1,2}/\partial t}{\sqrt{1+|\nabla\zeta_{1,2}|^2}}, \tag{8}$$

and the parameters b_o, b_d, and $\bar{b}_d$ are the corresponding Faraday coefficients.

We introduce the length scale $L=V\sigma_0/k_d^0$, the time scale $\tau=V\sigma_0/[b_d(k_d^0)^2]$, and the voltage scale V, and rewrite the system (1)–(5) in the following dimensionless form:

$$\nabla\cdot[f(E)\,\nabla\,\phi]=0, \tag{9}$$

$$z=\zeta_1(\mathbf{x},t):\quad -f(E)\partial_n\phi=\kappa_1 e^{\alpha(1-\phi)+\gamma_1 m_1}, \tag{10}$$

$$v_n^{(1)}=-\beta_1\kappa_1 e^{\alpha(1-\phi)+\gamma_1 m_1}, \tag{11}$$

$$z=\zeta_2(\mathbf{x},t):\quad -f(E)\partial_n\phi=e^{\alpha\phi+\gamma_2 m_2}-\kappa_2 e^{-\alpha\phi-\bar{\gamma}_2 m_2}, \tag{12}$$

$$v_n^{(2)}=-e^{\alpha\phi+\gamma_2 m_2}+\beta_2\kappa_2 e^{-\alpha\phi-\bar{\gamma}_2 m_2}, \tag{13}$$

where $f(E)=\sinh(\bar{p}E)/(\bar{p}E)$, $\kappa_1=k_o^0/k_d^0$, $\kappa_2=\bar{k}_d^0/k_d^0$, $\beta_1=b_o/b_d$, $\beta_2=\bar{b}_d/b_d$, $\alpha=V\alpha_e$, $(\gamma_{1,2},\bar{\gamma}_2)=(\gamma_{o,d},\bar{\gamma}_d)/L$, and $\bar{p}=pV/L$. For simplicity, we use the same notations for dimensionless coordinates, time, potential, field, and interface shapes.

III. STEADY-STATE SOLUTION

The problem (9)–(13) has the following steady-state solution corresponding to an oxide layer with a constant thickness l, moving with a constant speed v_s:

$$\zeta_{1s}=-v_s t,\quad \zeta_{2s}=l-v_s t,\quad \phi_s=-E_s(z-\zeta_{1s})+D_s, \tag{14}$$

where $D_s=1-\alpha^{-1}\ln[E_s f(E_s)/\kappa_1]$, the oxide layer thickness

$$l=\frac{1}{E_s}\left[1+\frac{1}{\alpha}\ln\left(\frac{\kappa_1}{\kappa_2}\frac{\beta_1-1}{1-\beta_2}\right)\right], \tag{15}$$

and the field E_s is the root of the equation

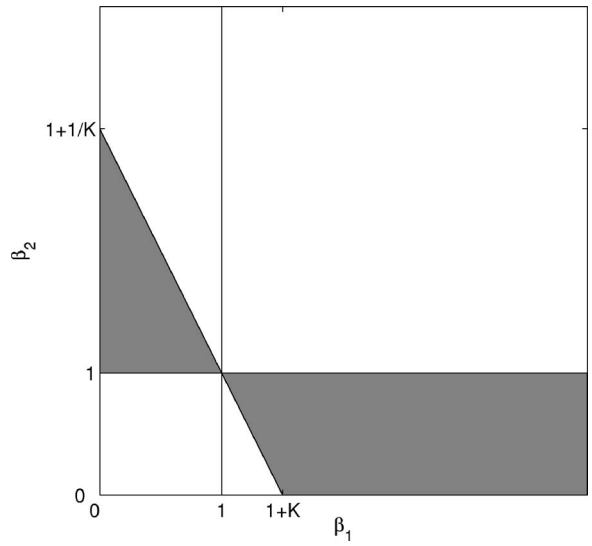

FIG. 2. Region of parameters (gray) where the steady-state solution (14)–(18) exists.

$$f(E_s)E_s = \sqrt{\kappa_2}\frac{|1-\beta_2|}{\sqrt{(\beta_1-1)(\beta_1-\beta_2)}}. \tag{16}$$

For $f(E)=\sinh(\bar{p}E)/(\bar{p}E)$, one obtains

$$E_s = \frac{1}{\bar{p}}\sinh^{-1}\left(\bar{p}\sqrt{\kappa_2}\frac{|1-\beta_2|}{\sqrt{(\beta_1-1)(\beta_1-\beta_2)}}\right). \tag{17}$$

The propagation speed of the oxide layer is

$$v_s = \beta_1 E_s f(E_s). \tag{18}$$

This steady-state solution exists only if $\beta_1>1$, $\beta_2<1$ or $\beta_1<1$, $\beta_2>1$, and if

$$\frac{\beta_1-1}{1-\beta_2} > \frac{\kappa_2}{\kappa_1}e^{-\alpha} \equiv K, \tag{19}$$

i.e., only for a certain relation between the Faraday coefficients of the interfacial electrochemical reactions and their rates. Regions in the parameter plane (β_1,β_2) where the stationary solution (14)–(18) exists are shown in Fig. 2. Also note that for $\kappa_2\to 0$ $(K\to 0)$, $l\to\infty$ and $E_s\to 0$.

One can see also that E_s is a decreasing function of the parameter $\bar{p}$ that characterizes the dependence of the oxide conductivity on electric field. The steady-state oxide layer thickness is an increasing function of this parameter.

IV. LINEAR STABILITY ANALYSIS

In this section we shall perform the linear stability analysis of the steady-state solution (14)–(18) corresponding to a uniformly propagating, planar oxide layer. Go over to the moving frame (notations for coordinates are kept the same), consider infinitesimal perturbations of the steady-state solution $\tilde{\phi}=\phi-\phi_s$, $\tilde{\zeta}_{1,2}=\zeta_{1,2}-\zeta_{1s,2s}$, and make the coordinate transformation

$$t\to\frac{t}{\alpha E_s f(E_s)\beta_1}, \quad z\to z\sqrt{1+E_s f'(E_s)/f(E_s)},$$

to obtain the following linearized problem:

$$\partial_{zz}\tilde{\phi}+\nabla^2\tilde{\phi}=0, \tag{20}$$

$$z=0: \quad F\partial_z\tilde{\phi}=\tilde{\phi}-E_s\tilde{\zeta}_1+\Gamma_1\nabla^2\tilde{\zeta}_1, \tag{21}$$

$$\partial_t\tilde{\zeta}_1=\tilde{\phi}-E_s\tilde{\zeta}_1+\Gamma_1\nabla^2\tilde{\zeta}_1, \tag{22}$$

$$z=\bar{l}: \quad F\partial_z\tilde{\phi}=B(-\tilde{\phi}+E_s\tilde{\zeta}_2)+\Gamma_2\nabla^2\tilde{\zeta}_2, \tag{23}$$

$$\partial_t\tilde{\zeta}_2=B'(-\tilde{\phi}+E_s\tilde{\zeta}_2)+\Gamma_2'\nabla^2\tilde{\zeta}_2, \tag{24}$$

where $\nabla^2=\partial_{xx}+\partial_{yy}$ is the two-dimensional Laplacian, and

$$F=\frac{F_s}{\alpha E_s}, \quad F_s=\sqrt{1+\frac{E_s f'(E_s)}{f(E_s)}}, \quad \bar{l}=\frac{l}{F_s},$$

$$B=\frac{1+\beta_2-2\beta_1}{\beta_2-1}, \quad B'=\frac{\beta_2-\beta_1+\beta_2(1-\beta_1)}{\beta_1(\beta_2-1)},$$

$$\Gamma_1=\frac{\gamma_1}{\alpha}, \quad \Gamma_2=\frac{\gamma_2(\beta_2-\beta_1)+\bar{\gamma}_2(1-\beta_1)}{\alpha(\beta_2-1)},$$

$$\Gamma_2'=\frac{\gamma_2(\beta_2-\beta_1)+\bar{\gamma}_2\beta_2(1-\beta_1)}{\alpha\beta_1(\beta_2-1)}.$$

Taking $\tilde{\phi}=\psi(z,t)e^{i\mathbf{k}\cdot\mathbf{x}}$, $\tilde{\zeta}_{1,2}=h_{1,2}(t)e^{i\mathbf{k}\cdot\mathbf{x}}$ yields $\psi(z)=C_k(t)\sinh kz+D_k(t)\cosh kz$, $(k=|\mathbf{k}|)$, and using the boundary conditions (22) and (24) one obtains for $\mathbf{h}=\binom{h_1}{h_2}$

$$\partial_t\mathbf{h}=A\mathbf{h}, \tag{25}$$

where the components a_{ij}, $i,j=1,2$, of the matrix A are

$$a_{11}=Fka_1,$$

$$a_{22}=B'[-a_2(\sinh k\bar{l}+Fk\cosh k\bar{l})+E_s]-\Gamma_2'k^2,$$

$$a_{12}=Fka_2,$$

$$a_{21}=-B'[a_1(\sinh k\bar{l}+Fk\cosh k\bar{l})+(E_s+\Gamma_1k^2)\cosh k\bar{l}],$$

$$a_1=-\Delta^{-1}(E_s+\Gamma_1k^2)(Fk\sinh k\bar{l}+B\cosh k\bar{l}),$$

$$a_2=\Delta^{-1}(BE_s-\Gamma_2k^2),$$

$$\Delta=(F^2k^2+B)\sinh k\bar{l}+Fk(1+B)\cosh k\bar{l}.$$

Take $\mathbf{h}=\mathbf{h}_0e^{\omega t}$ to obtain the dispersion relation in the form $\det(A-\omega I)=0$, where I is the identity matrix. This dispersion relation is a quadratic equation for ω with the coefficients depending on k and the physical parameters. It has two roots, corresponding to two modes,

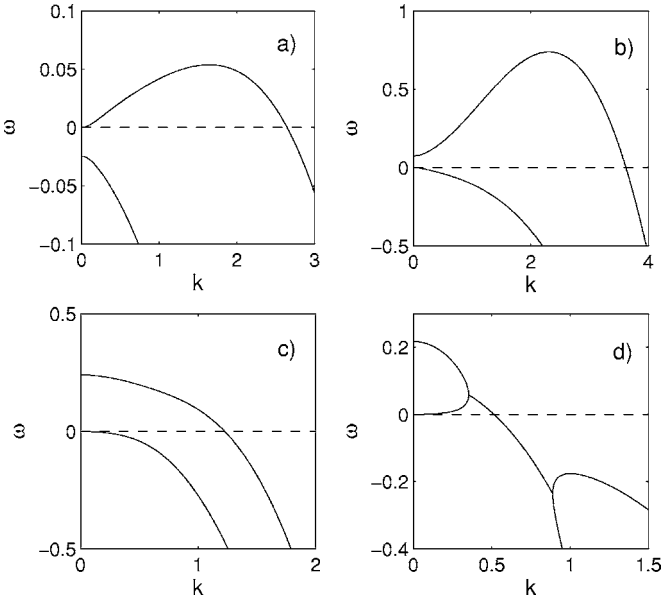

FIG. 3. Typical dispersion curves described by (26): (a) $\beta_1=1.1$, $\beta_2=0.3$, $\kappa_1=4.0$, $\kappa_2=3.0$, $\alpha=30.0$, $\gamma_1=0.5$, $\gamma_2=0.4$, $\bar{\gamma}_2=0.6$, $b=2.1$; (b) $\beta_1=0.5$, $\beta_2=3.0$, $\kappa_1=1.2$, $\kappa_2=0.2$, $\alpha=30.0$, $\gamma_1=0.5$, $\gamma_2=0.6$, $\bar{\gamma}_2=0.2$, $b=2.1$; (c) $\beta_1=0.3$, $\beta_2=1.5$, $\kappa_1=4.3$, $\kappa_2=3.3$, $\alpha=20.0$, $\gamma_1=1.5$, $\gamma_2=0.75$, $\bar{\gamma}_2=0.7$, $b=1.5$; (d) $\beta_1=0.3$, $\beta_2=1.5$, $\kappa_1=5.3$, $\kappa_2=3.0$, $\alpha=20.0$, $\gamma_1=0.5$, $\gamma_2=0.4$, $\bar{\gamma}_2=0.8$, $b=2.1$.

$$\omega_{\pm}(k) = T/2 \pm \sqrt{T^2/4 - D}, \tag{26}$$

where $T=\mathrm{Tr}(A)$ and $D=\det(A)$. The mode ω_- describes zigzag perturbations of the oxide layer shape, with $\omega_-(0)=0$, which corresponds to the zero mode associated with the translation symmetry of the system. The mode ω_+ corresponds to varicose perturbations, and

$$\omega_+(0) = 2E_s \frac{(\beta_1-1)(\beta_1-\beta_2)}{\beta_1(\beta_2-1)} \frac{1}{1+B(1+\bar{l}/F)}. \tag{27}$$

Since for the values of $\beta_{1,2}$, for which the stationary solution (14)–(18) exists (see Fig. 2), $B>0$, then $\omega_+(0)<0$ for $\beta_1>1$, $\beta_2<1$ and $\omega_+(0)>0$ for $\beta_1<1$, $\beta_2>1$. In the latter case, a planar oxide layer is unstable with respect to spatially homogeneous perturbations and will either continuously shrink or expand.

Some typical dispersion curves, $\omega_+(k)$ and $\omega_-(k)$, are shown in Fig. 3. Note that for some parameter values an oscillatory branch can appear for some wave numbers. However, since $T>0$ for $\beta_1>1$ and $T<0$ for $\beta_1<1$, the long-wave oscillatory instability (for $k\to 0$) is impossible in this system.

We shall further be interested in the case when the varicose mode is damped, i.e., when $\beta_1>1$, $\beta_2<1$. The zigzag mode $\omega_-(k)$ becomes unstable if $(\partial^2\omega_-/\partial k^2)_{k=0}>0$, i.e., for

$$l > \alpha \frac{(\beta_1-1)(\beta_1-\beta_2)(\gamma_2-\bar{\gamma}_2)}{\beta_1(1+\beta_2)-2\beta_2}. \tag{28}$$

Since the denominator of (28) is positive, one concludes that if $\gamma_2<\bar{\gamma}_2$ the oxide layer is always unstable with respect to the zigzag mode, while if $\gamma_2>\bar{\gamma}_2$ there is a threshold for the instability given by (28). One can see that the oxide layer becomes unstable when its steady-state thickness, determined by (15) and (16), exceeds a certain critical value that depends on the Faraday coefficients and the activation capillary lengths characterizing the oxide dissolution (and inverse) reactions. In terms of dimensional parameters, the instability occurs when the steady-state oxide layer thickness l^* exceeds the following threshold:

$$l^* > \frac{eV}{2k_BT} \frac{(b_o-b_d)(b_o-\bar{b}_d)(\gamma_d-\bar{\gamma}_d)}{b_o(b_d+\bar{b}_d)-2b_d\bar{b}_d}. \tag{29}$$

For $V=30$ V, $T=300$ K, and $\gamma_d-\bar{\gamma}_d\approx 1-10$ nm, one obtains $l^*\approx 20-200$ nm, which is in accordance with experimental observations for aluminum oxide. One can see that the critical thickness of the oxide layer is proportional to the applied voltage. Note that the activation capillary length of the metal oxidation reaction, γ_o, does not affect the stability conditions; it only contributes to stabilization of the short-wave modes, i.e., to the wavelength selection mechanism. Note also that the dependence of the oxide conductivity on the electric field, characterized by the parameter $\bar{p}$, has a destabilizing effect, since the equilibrium value of the oxide layer increases with the increase of $\bar{p}$.

V. WEAKLY NONLINEAR ANALYSIS

As one can see from the linear stability analysis, under certain conditions the oxide layer can become unstable with respect to perturbations whose wave number is less than the cutoff wave number, $k<k_*$. We are interested in the case when the varicose mode is damped, and the zigzag mode is characterized by the dependence $\omega(k)$ shown in Fig. 3(a). Near the instability threshold, $k_*\ll 1$, and one can use a multiple-scale analysis in order to derive a nonlinear evolution equation that governs the system behavior in this case. This derivation is standard and the details can be found elsewhere [30,31]. Here we reproduce only the main steps.

Consider the parameters of the system to be such that the oxide layer described by the steady-state solution (14)–(18) is weakly unstable (near the instability threshold), so that the dispersion relation for the unstable mode can be expanded as

$$\omega = ak^2 - bk^4, \tag{30}$$

where a and b are positive,

$$a = \frac{1}{2}\left(\frac{\partial^2\omega}{\partial k^2}\right)_{k=0} = O(\epsilon^2), \quad b = -\frac{1}{24}\left(\frac{\partial^4\omega}{\partial k^4}\right)_{k=0} = O(1).$$

Here, the small parameter $\epsilon\ll 1$ is proportional to $\sqrt{P-P_c}$, where the parameter P stands for any of the parameters in the problem, and P_c is the critical value of P corresponding to the onset of the instability. In this case the range of the wave numbers Δk corresponding to the unstable modes ($\omega>0$) is small, $\Delta k\sim\epsilon\ll 1$, and the maximal growth rate $\omega_{max}\sim\epsilon^4$.

Go over to the moving frame and introduce the moving frame coordinate, $\tilde{z}=z+v_0t$, the long-scale coordinates in the

plane parallel to the MO and OE interfaces, $\mathbf{X}=\epsilon\mathbf{x}$, and the slow time variable, $T=\epsilon^4 t$, and consider perturbations of the electric potential and perturbations of the two planar interfaces in the form of the expansions

$$\phi = \phi^{(0)}(\tilde{z}) + \epsilon^2\phi^{(1)}(\tilde{z},\mathbf{X},T) + \epsilon^4\phi^{(2)}(\tilde{z},\mathbf{X},T) + \epsilon^6\phi^{(3)}(\tilde{z},\mathbf{X},T) + \cdots, \tag{31}$$

$$\boldsymbol{\zeta} = \boldsymbol{\zeta}^{(0)} + \epsilon^2\boldsymbol{\zeta}^{(1)}(\mathbf{X},T) + \epsilon^4\boldsymbol{\zeta}^{(2)}(\mathbf{X},T) + \epsilon^6\boldsymbol{\zeta}^{(3)}(\mathbf{X},T) + \cdots, \tag{32}$$

where $\boldsymbol{\zeta}=\binom{\zeta_1}{\zeta_2}$ and $\boldsymbol{\zeta}^{(0)}=\binom{0}{l}$.

Substitute the expansions (31) and (32) into the problem (9)–(13), to obtain a sequence of linear problems in even orders of the small parameter ϵ. The problem at order ϵ^2 is

$$A_0\boldsymbol{\zeta}^{(1)} = 0, \tag{33}$$

where $A_0=\lim_{k\to 0} A$, $\det A_0=0$. Therefore, $\boldsymbol{\zeta}^{(1)}$ is the null vector of A_0,

$$\boldsymbol{\zeta}^{(1)} = \begin{pmatrix} 1 \\ 1 \end{pmatrix} U(\mathbf{X},T), \tag{34}$$

where $U(\mathbf{X},T)$ is an as yet unknown function.

The problem at order ϵ^4 is

$$A_0\boldsymbol{\zeta}^{(2)} = \mathbf{u}\nabla^2 U, \tag{35}$$

where the components of the vector $\mathbf{u}$ are cumbersome functions of the system parameters. The solvability condition of the problem (35) gives the condition for the instability threshold, $2a=\partial^2\omega/\partial k^2=0$, which is identically satisfied since the parameters have been chosen such that $a=O(\epsilon^2)$; the right-hand side of (35) must be carried out to the next order.

The problem at order ϵ^6 is

$$A_0\boldsymbol{\zeta}^{(3)} = \mathbf{u}\nabla^2 U + \mathbf{v}(\boldsymbol{\nabla} U)^2 + \mathbf{w}\nabla^4 U + \mathbf{s}U_T, \tag{36}$$

where the components of the vectors $\mathbf{u}$, $\mathbf{v}$, $\mathbf{w}$, and $\mathbf{s}$ are cumbersome functions of the system parameters.

The solvability condition for the problem at order ϵ^6 gives the following evolution equation for the function $U(\mathbf{X},T)$:

$$U_T + a\nabla^2 U + b\nabla^4 U - \frac{v_0}{2}(\boldsymbol{\nabla} U)^2 = 0, \tag{37}$$

where $\boldsymbol{\nabla}$ is the gradient operator acting on the long-scale coordinates $\mathbf{X}$, a and b are defined in (30), and v_0 is the dimensional speed of the propagating oxide layer in the steady state. The nonlinear term describes the correction of the interface velocity projection on the z direction for a slightly slant interface. Equation (37) is the well-known Kuramoto-Sivashinsky equation that describes weakly nonlinear evolution in many systems with translation invariance [31,32], characterized by a monotonic instability with the long-wave spectrum (30), such as the thermodiffusive instability of a flame front [33], the liquid film flow instability [34,35], as well as morphological instabilities of crystallization fronts [36–38]. It has been extensively studied (see, e.g., [39]) and is known to exhibit cellular structures that vary slowly in time and space in a chaotic manner. In our case, it describes the nonlinear evolution of an unstable oxide layer near the instability threshold, when the perturbation wavelength is large compared to the oxide layer thickness. The solution of this equation describes the shape of the MO and OE interfaces. A typical solution of Eq. (37) in a particular moment of time is shown in Fig. 4. It strongly resembles the initial stage of evolution of irregular pores in anodic aluminum oxide observed in [10].

VI. STRONGLY NONLINEAR LONG-WAVE EQUATIONS

The Kuramoto-Sivashinsky equation discussed above describes the system nonlinear evolution only near the instability threshold, when $P-P_c\sim\epsilon^2, k\sim\epsilon$, $\omega\sim\epsilon^4$, and the perturbations of the interface shape are small, $\zeta_{1,2}\sim\epsilon^2$. For certain parameter values it is possible that the instability remains long wave (the cutoff wave number is small) and the evolution still remains slow far from the instability threshold. In this case it is possible to derive strongly nonlinear evolution equations for the shapes of the interfaces $\zeta_{1,2}$ in the long-wave approximation, such that $\zeta_{1,2}\sim O(1)$.

Thus, we assume that the parameters of the system are such that the typical wavelength of the interfacial perturbations is much larger than the oxide layer thickness. For the sake of simplicity we neglect the dependence of the oxide conductivity on the electric field, thus assuming $f(E)\equiv 1$. Consider the problem (9)–(13), introduce the long-scale in-plane coordinates $\mathbf{X}=\epsilon\mathbf{x}$, and the slow time $T=\epsilon^2 t$, consider $\zeta_{1,2}=\zeta_{1,2}(t,T,\mathbf{X})$, $\phi=\phi_0(z,\mathbf{X},t,T)+\epsilon^2\phi_1(z,\mathbf{X},t,T)+\cdots$, and use the transformations $\partial_t\to\partial_t+\epsilon^2\partial_T$, $\boldsymbol{\nabla}\to\epsilon\boldsymbol{\nabla}$, where the gradient operator acts on the in-plane long-scale coordinates. Then, from (9)–(13) one obtains the hierarchy of problems at different orders of ϵ.

The problem at zero order reads

$$\partial_{zz}\phi_0 = 0, \tag{38}$$

$$z=\zeta_1: \quad -\partial_z\phi_0 = \kappa_1 e^{\alpha(1-\phi_0)}, \tag{39}$$

$$\partial_t\zeta_1 = \beta_1\partial_z\phi_0, \tag{40}$$

$$z=\zeta_2: \quad -\partial_z\phi_0 = e^{\alpha\phi_0} - \kappa_2 e^{-\alpha\phi_0}, \tag{41}$$

$$\partial_t\zeta_2 = -e^{\alpha\phi_0} + \beta_2\kappa_2 e^{-\alpha\phi_0}. \tag{42}$$

From (38)–(42) one obtains

$$\phi_0 = -E_0 z + \Phi_0, \quad \Phi_0 = 1 + E_0\zeta_1 - \frac{1}{\alpha}\ln\frac{E_0}{\kappa_1}, \tag{43}$$

where the electric field E_0 is determined as the root of the following transcendental equation:

$$E_0^2 = \frac{\kappa_1^2\exp\{\alpha[1-E_0(\zeta_2-\zeta_1)]\}}{\kappa_1+\kappa_2\exp\{-\alpha[1-E_0(\zeta_2-\zeta_1)]\}}, \tag{44}$$

and the motion of the two interfaces is described by the following system:

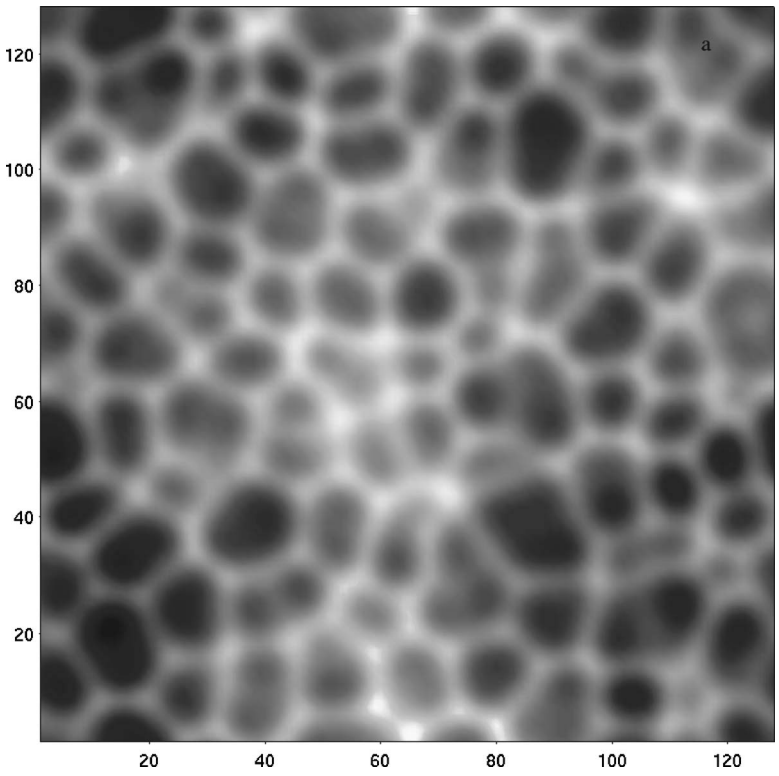

FIG. 4. Numerical solution of Eq. (37) in a particular moment of time.

$$\partial_t \zeta_1 = -\beta_1 E_0 \equiv F_1^{(0)}(E_0), \quad \partial_t \zeta_2 = -\left(E_0' - \frac{\beta_2 \kappa_2}{E_0'}\right) \equiv F_2^{(0)}(E_0), \tag{45}$$

where

$$E_0' = E_0/2 + \sqrt{E_0^2/4 + \kappa_2}. \tag{46}$$

The problem at order $O(\epsilon^2)$ reads

$$\partial_{zz}\phi_1 = -\nabla^2 \phi_0, \tag{47}$$

$$z = \zeta_1: \quad -\partial_z \phi_1 + \boldsymbol{\nabla}\zeta_1 \cdot \boldsymbol{\nabla}\phi_0 = \kappa_1 e^{\alpha(1-\phi_0)}\left(\frac{1}{2}(\boldsymbol{\nabla}\zeta_1)^2 - \alpha\phi_1 - \gamma_1 \nabla^2 \zeta_1\right), \tag{48}$$

$$\partial_T \zeta_1 = \beta_1(\partial_z \phi_1 - \boldsymbol{\nabla}\zeta_1 \cdot \boldsymbol{\nabla}\phi_0), \tag{49}$$

$$z = \zeta_2: \quad -\partial_z \phi_1 + \boldsymbol{\nabla}\zeta_2 \cdot \boldsymbol{\nabla}\phi_0 = e^{\alpha\phi_0}\left(\frac{1}{2}(\boldsymbol{\nabla}\zeta_2)^2 + \alpha\phi_1 - \gamma_2 \nabla^2 \zeta_2\right) - \kappa_2 e^{-\alpha\phi_0}\left(\frac{1}{2}(\boldsymbol{\nabla}\zeta_2)^2 - \alpha\phi_1 + \bar{\gamma}_2 \nabla^2 \zeta_2\right), \tag{50}$$

$$\partial_T \zeta_2 = -e^{\alpha\phi_0}\left(\frac{1}{2}(\boldsymbol{\nabla}\zeta_2)^2 + \alpha\phi_1 - \gamma_2 \nabla^2 \zeta_2\right) + \beta_2 \kappa_2 e^{-\alpha\phi_0}\left(\frac{1}{2}(\boldsymbol{\nabla}\zeta_2)^2 - \alpha\phi_1 + \bar{\gamma}_2 \nabla^2 \zeta_2\right). \tag{51}$$

One obtains

$$\phi_1 = -E_1 z + \Phi_1 + \nabla^2 E_0 \frac{z^3}{6} - \nabla^2 \Phi_0 \frac{z^2}{2}, \tag{52}$$

where E_1 and Φ_1 satisfy the following system of linear equations:

$$E_1(1 - \alpha E_0 \zeta_1) + \alpha E_0 \Phi_1 = \boldsymbol{\nabla}\cdot\left(\frac{1}{2}\zeta_1^2 \boldsymbol{\nabla} E_0 - \zeta_1 \boldsymbol{\nabla}\Phi_0\right) + \frac{1}{2}E_0(\boldsymbol{\nabla}\zeta_1)^2 + E_0\left[\alpha\left(-\frac{1}{6}\zeta_1^3 \nabla^2 E_0 + \frac{1}{2}\zeta_1^2 \nabla^2 \Phi_0\right) - \gamma_1 \nabla^2 \zeta_1\right], \tag{53}$$

$$E_1(1 + \alpha E_0'' \zeta_2) - \alpha E_0'' \Phi_1 = \boldsymbol{\nabla}\cdot\left(\frac{1}{2}\zeta_2^2 \boldsymbol{\nabla} E_0 - \zeta_2 \boldsymbol{\nabla}\Phi_0\right) + \frac{1}{2}E_0(\nabla\zeta_2)^2 + E_0''\left[\alpha\left(\frac{1}{6}\zeta_2^3 \nabla^2 E_0 - \frac{1}{2}\zeta_2^2 \nabla^2 \Phi_0\right) - \gamma_2' \nabla^2 \zeta_2\right], \tag{54}$$

where

$$E_0'' = E_0' + \frac{\kappa_2}{E_0'}, \quad \gamma_2' = \frac{1}{E_0''}\left(\gamma_2 E_0' + \bar{\gamma}_2 \frac{\kappa_2}{E_0'}\right).$$

For the evolution of the interfaces on the slow time scale one obtains

$$\partial_T \zeta_1 = \beta_1\left[-E_1 + \boldsymbol{\nabla}\cdot\left(\frac{1}{2}\zeta_1^2 \boldsymbol{\nabla} E_0 - \zeta_1 \boldsymbol{\nabla}\Phi_0\right)\right] \equiv F_1^{(1)}(E_0, \zeta_1, \zeta_2), \tag{55}$$

$$\partial_T \zeta_2 = -\alpha\left(E_0' + \frac{\beta_2\kappa_2}{E_0'}\right)\left(-E_1\zeta_2 + \Phi_1 + \frac{1}{6}\zeta_2^3\nabla^2 E_0 - \frac{1}{2}\zeta_2^2\nabla^2\Phi_0\right) - \left(E_0' - \frac{\beta_2\kappa_2}{E_0'}\right)\frac{1}{2}(\nabla\zeta_2)^2 + \left(E_0'\gamma_2 + \frac{\beta_2\kappa_2}{E_0'}\bar{\gamma}_2\right)\nabla^2\zeta_2 \equiv F_2^{(1)}(E_0,\zeta_1,\zeta_2). \quad (56)$$

Finally, introducing a composed time variable $\tau = t + \epsilon^2 T$, we combine Eqs. (45), (55), and (56) to obtain a system of long-wave, strongly nonlinear equations for the shapes of the MO and OE interfaces,

$$\partial_\tau \zeta_1 = F_1^{(0)}(E_0) + F_1^{(1)}(E_0,\zeta_1,\zeta_2), \quad (57)$$

$$\partial_\tau \zeta_2 = F_2^{(0)}(E_0) + F_2^{(1)}(E_0,\zeta_1,\zeta_2), \quad (58)$$

where the functions $F_{1,2}^{(0,1)}$ are defined in Eqs. (45), (55), and (56), E_0 is the solution of Eq. (44) which depends on the local oxide layer thickness $\zeta_2 - \zeta_1$, and E_1 and Φ_1 are the solutions of the system (53) and (54).

The system (57) and (58) describes the strongly nonlinear evolution of the MO and OE interfaces in the long-wave approximation, when the oxide layer thickness is much smaller than the cutoff wavelength of the instability. One can see that it is very cumbersome and difficult to analyze. It simplifies significantly in the case when the rate of the oxide reformation reaction can be neglected. For $\kappa_2 = 0$ one obtains $E_0' = E_0$, and

$$\partial_\tau \zeta_1 = -\beta_1 E_1 + \beta_1 \nabla \cdot \left(\frac{1}{2}\zeta_1^2 \nabla E_0 - \zeta_1 \nabla \Phi_0\right) - \beta_1 E_0, \quad (59)$$

$$\partial_\tau \zeta_2 = -E_1 + \nabla \cdot \left(\frac{1}{2}\zeta_2^2 \nabla E_0 - \zeta_2 \nabla \Phi_0\right) - E_0, \quad (60)$$

where E_1 is determined by

$$E_1[2 + \alpha E_0(\zeta_2 - \zeta_1)] = \nabla \cdot \left(\frac{1}{2}(\zeta_1^2 + \zeta_2^2)\nabla E_0 - (\zeta_1 + \zeta_2)\nabla \Phi_0\right) + \frac{1}{2}E_0[(\nabla\zeta_1)^2 + (\nabla\zeta_2)^2] + \alpha E_0\left(\frac{1}{6}(\zeta_2^3 - \zeta_1^3)\nabla^2 E_0 - \frac{1}{2}(\zeta_2^2 - \zeta_1^2)\nabla^2\Phi_0\right) - E_0(\gamma_1\nabla^2\zeta_1 + \gamma_2\nabla^2\zeta_2), \quad (61)$$

Φ_0 is defined by (43), and E_0 is the root of the transcendental equation

$$E_0 = \sqrt{\kappa_1}\exp\left(\frac{\alpha}{2}[1 - E_0(\zeta_2 - \zeta_1)]\right). \quad (62)$$

We shall further concentrate on solving the system (59) and (60).

We have represented the system (59) and (60) in the form $\partial_\tau \boldsymbol{\zeta} = L\boldsymbol{\zeta} + (N-L)\boldsymbol{\zeta}$, where $\boldsymbol{\zeta} = \begin{pmatrix}\zeta_1\\ \zeta_2\end{pmatrix}$, N is the right-hand side of (59) and (60), and L is N linearized around an initial value of the oxide layer thickness, l. We have solved this system numerically, by a pseudospectral method, with time integration in the Fourier space, using the Crank-Nicolson scheme for the linear operator L and the Adams-Bashforth scheme for the nonlinear operator $N-L$, starting from small-amplitude random perturbations of the two planar interfaces, with the initial thickness of the oxide layer l_0. At each time step Eq. (62) was solved numerically, and the relations

$$\frac{\partial E_0}{\partial l} = -\frac{\alpha E_0^2}{2 + \alpha l E_0}, \quad \frac{\partial^2 E_0}{\partial l^2} = \frac{2\alpha^2 E_0^3(3 + \alpha l E_0)}{(2 + \alpha l E_0)^3},$$

where $l = \zeta_2 - \zeta_1$, were used.

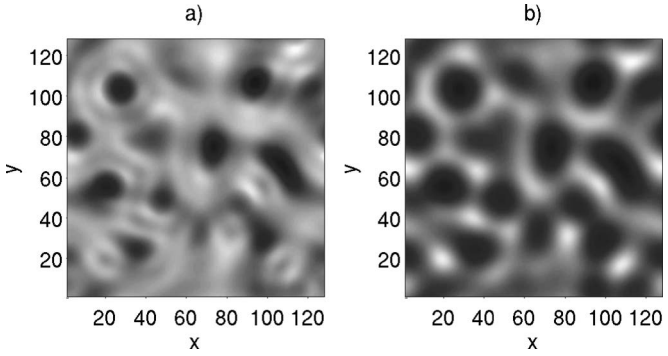

FIG. 5. Numerical solution of the system (59) and (60) at a particular moment of time showing developed pores: (a) MO interface $\zeta_1(x,y)$; (b) OE interface $\zeta_2(x,y)$. Here $\beta_1 = 1.01$, $\kappa_1 = 10^{-5}$, $\alpha = 10.0$, $\gamma_1 = 0.5$, $\gamma_2 = 20.5$, and the initial thickness of the oxide layer is $l_0 = 0.1$.

Figure 5 shows the numerical solution of the system (59) and (60) at a particular moment of time corresponding to well-developed pores. One can see the formation of spatially irregular array of deep pores in the oxide layer that start at the OE interface. The shape of the MO interface follows the spatial pattern of pores in the oxide, however, with the considerably smaller amplitude, which is consistent with experimental observations.

The dynamics of the pore formation is shown in Fig. 6 (for computations performed in a domain twice larger than that shown in Fig. 5).

We also note that the pores have a parabolic shape in the vicinity of the tip. We show below that in the particular case of $\beta_1 = 1$, i.e., when the Faraday coefficients of the oxidation and dissolution reactions are equal, the system (59) and (60) has a self-similar solution in the form of a propagating pore with a paraboloid shape. Indeed, for $\beta_1 = 1$ one obtains that the local thickness of the oxide layer, $\zeta_2 - \zeta_1$, does not depend on time. Assume $\zeta_2(\mathbf{x},\tau) - \zeta_1(\mathbf{x},\tau) = l = \text{const}$; then Eq. (59) for ζ_1 is reduced to

$$\partial_\tau \zeta_1 = a\nabla^2\zeta_1 - b(\nabla\zeta_1)^2 - E_0, \quad (63)$$

where

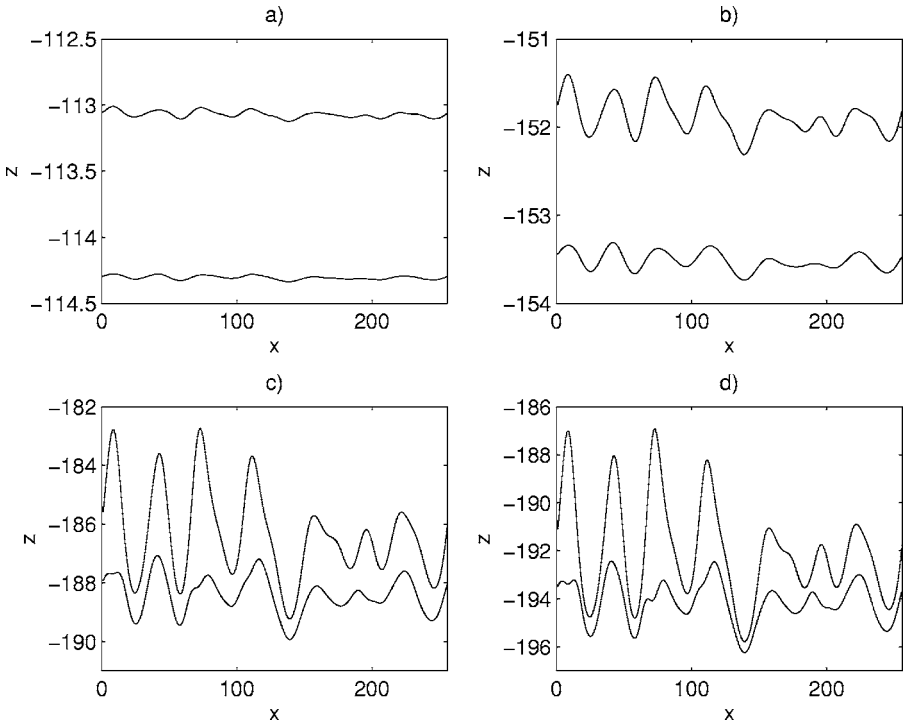

FIG. 6. Dynamics of the pore formation: numerical solutions of the system (59) and (60) at different moments of time, corresponding to a particular cross section of the two interfaces along the x direction. Lower curve, MO interface ζ_1; upper curve, OE interface ζ_2. The parameters are the same as those corresponding to Fig. 5.

$$a = \frac{1}{2}E_0 l + \frac{E_0(\gamma_1 + \gamma_2)}{2 + \alpha E_0 l}, \quad b = \frac{E_0(1 + \alpha E_0 l)}{2 + \alpha E_0 l}.$$

Use the ansatz $\zeta_1 = A(\tau)r^2 + B(\tau) - E_0\tau$ $(r^2 = x^2 + y^2)$ to obtain from Eq. (63) a system of differential equations for A and B:

$$\frac{dA}{d\tau} = -4bA^2, \quad \frac{dB}{d\tau} = 4aA,$$

the solution of which gives the following solution for ζ_1:

$$\zeta_1 = \frac{r^2}{4b\tau + c} + \frac{a}{b}\ln(4b\tau + c) - E_0\tau + \text{const}, \qquad (64)$$

where c is the initial pore "width." Solution (64) describes a pore with a paraboloid shape. The pore tip propagates with the speed $-E_0 + 4a/(4b\tau + c)$, approaching the constant speed E_0, and the pore widens with time. Note also that Eq. (63) is the well-known Burgers equation that can be solved exactly using the Cole-Hopf transformation which reduces Eq. (63) to the diffusion equation; solution (64) can also be obtained this way.

Note, however, that the long-wave system (59) and (60) gives only a qualitative picture of the evolution of deep pores. As one can see from Fig. 6, at late stages, when the pores become very deep and also grow deeper in the metal, the oxide layer thickness at the pore wall may become very thin and cross zero. This is an artifact of the long-wave approximation which breaks down when the pore slope becomes large enough; Eqs. (59) and (60) cannot describe further evolution of the system. Thus, although the system (59) and (60) gives a correct qualitative picture of the pore formation in an oxide layer, a fully nonlinear treatment is necessary for the description of the evolution of deep pores. Also note that the present theory does not consider such important processes as mass transport in electrolyte, especially inside the electrical double layer and inside the pores, and details of electrochemical kinetics at the interfaces. A comprehensive theory of self-assembly of porous structures in anodic oxides would require a detailed consideration of such processes which still remains to be done.

ACKNOWLEDGMENTS

This work was supported by the NSF Grant No. DMS-0204643. C. S. also acknowledges support of the NSF IGERT.

[1] J. P. O'Sullivan and G. C. Wood, Proc. R. Soc. London, Ser. A **317**, 511 (1970).
[2] G. E. Thompson, Thin Solid Films **297**, 192 (1997).
[3] R. Beranek, H. Hildebrand, and P. Schmuki, Electrochem. Solid-State Lett. **6**, B12 (2003).
[4] D. Gong, C. A. Grimes, O. K. Varghese, W. C. Hu, R. S. Singh, Z. Chen, and E. C. Dickey, J. Mater. Res. **16**, 3331 (2001).
[5] J. M. Macak, H. Tsuchiya, and P. Schmuki, Angew. Chem., Int. Ed. **44**, 2100 (2005).
[6] H. C. Shin, J. Dong, and M. L. Liu, Adv. Mater. (Weinheim, Ger.) **16**, 237 (2004).
[7] H. Masuda and K. Fukuda, Science **268**, 1466 (1995).

[8] H. Masuda, H. Yamada, M. Satoh, H. Asoh, M. Nakao, and T. Tamamura, Appl. Phys. Lett. **71**, 2770 (1997).
[9] A. P. Li, F. Muller, A. Birner, K. Nielsch, and U. Gosele, J. Appl. Phys. **84**, 6023 (1998).
[10] F. Y. Li, L. Zhang, and R. M. Metzger, Chem. Mater. **10**, 2470 (1998).
[11] A. Huczko, Appl. Phys. A: Mater. Sci. Process. **70**, 365 (2000).
[12] J. Choi, Y. Luo, R. B. Wehrspohn, R. Hillebrand, J. Schilling, and U. Gosele, J. Appl. Phys. **94**, 4757 (2003).
[13] G. S. Cheng and M. Moskovits, Adv. Mater. (Weinheim, Ger.) **14**, 1567 (2002).
[14] G. Schmid, J. Mater. Chem. **12**, 1231 (2002).
[15] H. Asoh, K. Nishio, M. Nakao, T. Tamamura, and H. Masuda, J. Electrochem. Soc. **148**, B152 (2001).
[16] K. Nielsch, J. Choi, K. Schwirn, R. B. Wehrspohn, and U. Gosele, Nano Lett. **2**, 677 (2002).
[17] O. Jessensky, F. Muller, and U. Gosele, Appl. Phys. Lett. **72**, 1173 (1998).
[18] V. Parkhutik, Solid-State Electron. **43**, 1121 (1999).
[19] M. Rauscher and H. Spohn, Phys. Rev. E **64**, 031604 (2001).
[20] S. Frey, B. Gresillon, F. Ozanam, J.-N. Chazalviel, J. Cartensen, H. Föll, and R. B. Wehrspohn, Electrochem. Solid-State Lett. **8**, B25 (2005).
[21] V. P. Parkhutik and V. I. Shershulsky, J. Phys. D **25**, 1258 (1992).
[22] S. K. Thamida and H. C. Chang, Chaos **12**, 240 (2002).
[23] G. K. Singh, A. A. Golovin, I. S. Aranson, and V. Vinokur, Europhys. Lett. **70**, 836 (2005).
[24] G. K. Singh, A. A. Golovin, and I. S. Aranson, Phys. Rev. B **73**, 205422 (2006).
[25] J. O'M. Bockris and A. K. N. Reddy, *Modern Electrochemistry* (Plenum Press, New York, 1970).
[26] Y. Kang and J. Jorne, J. Electrochem. Soc. **140**, 2258 (1993).
[27] A. Valance, Phys. Rev. B **52**, 8323 (1995).
[28] W. Guo and D. Johnson, Phys. Rev. B **67**, 075411 (2003).
[29] J.-N. Chazalviel, R. B. Wehrspohn, and F. Ozanam, Mater. Sci. Eng., B **69-70**, 1 (2000).
[30] B. J. Matkowsky and G. I. Sivashinsky, SIAM J. Appl. Math. **37**, 686 (1979).
[31] A. A. Nepomnyashchy, Physica D **86**, 90 (1985).
[32] Y. Kuramoto and T. Tsuzuki, Prog. Theor. Phys. **55**, 536 (1976).
[33] G. I. Sivashinsky, Acta Astron. **4**, 1177 (1977).
[34] A. A. Nepomnyashchy, Fluid Dyn. **9**, 354 (1974).
[35] G. M. Homsy, Lect. Appl. Math. **15**, 191 (1974).
[36] A. Novick-Cohen, Physica D **26**, 403 (1987).
[37] M. L. Frankel, Physica D **27**, 260 (1987).
[38] A. Umantsev and S. H. Davis, Phys. Rev. A **45**, 7195 (1992).
[39] T. Bohr, M. H. Jensen, G. Paladin, and A. Vulpiani, *Dynamical Systems Approach to Turbulence* (Cambridge University Press, Cambridge, U.K., 1998).